



Evaluation of ECG-Gated, High-Pitch Thoracoabdominal Angiographies With Dual-Source Photon-Counting Detector Computed Tomography

K. Rippel, MD¹ , J. Luitjens, MD¹, O. Habeeballah, MD¹, C. Scheurig-Muenkler, MHBA¹ , Stefanie Bette, MD¹, Franziska Braun, MD¹, T. J. Kroencke, MBA^{1,2} , F. Schwarz, MD^{3*}, and J. A. Decker, MD^{1*}

Abstract

Purpose: The aim of this study was to evaluate the radiation dose, image quality, and the potential of virtual monoenergetic imaging (VMI) reconstructions of high-pitch computed tomography angiography (CTA) of the thoracoabdominal aorta on a dual-source photon-counting detector–CT (PCD-CT) in comparison with an energy-integrating detector–CT (EID-CT), with a special focus on low-contrast attenuation. **Methods:** Consecutive patients being referred for an electrocardiogram (ECG)-gated, high-pitch CTA of the thoracoabdominal aorta prior to transcatheter aortic valve replacement (TAVR), and examined on the PCD-CT, were included in this prospective single-center study. For comparison, a retrospective patient group with ECG-gated, high-pitch CTA examinations of the thoracoabdominal aorta on EID-CT with a comparable scan protocol was matched for gender, body mass index, height, and age. Virtual monoenergetic imaging reconstructions from 40 to 120 keV were performed. Enhancement and noise were measured in 7 vascular segments and the surrounding air as mean and standard deviation of CT values. The radiation dose was noted and signal-to-noise ratio (SNR) and contrast-to-noise ratio (CNR) were calculated. Finally, a subgroup analysis was performed, comparing VMI reconstructions from 40 keV to 70 keV in patients with at least a 50% decrease in contrast attenuation between the ascending aorta and femoral arteries. **Results:** Fifty patients (mean age 77.0 ± 14.5 years; 31 women) were included. The radiation dose was significantly lower on the PCD-CT (4.2 ± 1.4 vs. 7.2 ± 2.2 mGy; $p < 0.001$). With increasing keV, vascular noise, SNR, and CNR decreased. Intravascular attenuation was significantly higher on VMI at levels from 40 to 65, compared with levels of 120 keV ($p < 0.01$ and $p < 0.005$, respectively). On the PCD-CT, SNR was significantly higher in keV levels 40 and 70 (all $p < 0.001$), and CNR was higher at keV levels 40 and 45 (each $p < 0.001$), compared with scans on the EID-CT. At VMI ≤ 60 keV, image noise was also significantly higher than that in the control group. The subgroup analysis showed a drastically improved diagnostic performance of the low-keV images in patients with low-contrast attenuation. **Conclusion:** The ECG-gated CTA of the thoracoabdominal aorta in high-pitch mode on PCD-CT have significantly lower radiation dose and higher objective image quality than EID-CT. In addition, low-keV VMI can salvage suboptimal contrast studies, further reducing radiation dose by eliminating the need for repeat scans.

Clinical Impact

ECG-gated CT-angiographies of the thoracoabdominal aorta can be acquired with a lower radiation dose and a better image quality by using a dual-source photon-counting detector CT. Furthermore, the inherent spectral data offers the possibility to improve undiagnostic images and thus saves the patient from further radiation and contrast application.

Keywords

photon-counting detector–CT, energy-integrating detector–CT, high-pitch ECG-gated aortic CT angiographies, virtual monoenergetic imaging, low-contrast attenuation scans

Introduction

Transcatheter aortic valve replacement (TAVR) is a standard procedure for the treatment of aortic valve stenosis.

A computed tomography angiography (CTA) of the thoracoabdominal aorta is performed usually as an electrocardiogram (ECG)-gated high-pitch CTA to assess the approach through the femoral artery and the anatomy of

the heart. This information is essential for the interventionalists and surgeons to plan the procedure. The potential radiation dose reduction of high-pitch examinations has been demonstrated in many studies.^{1,2} Low-keV CTAs have also been evaluated to further reduce the radiation dose.^{3,4} In addition, the possibility of improving diagnostic efficiency by using spectral images from a dual-source CT was investigated.^{5,6} However, when looking at the low-keV reconstructions of the virtual monoenergetic imaging (VMI), the increasing noise level became particularly apparent.⁷ Even with optimized iterative reconstructions, this remains an issue.⁸

Recently, photon-counting detector-CT (PCD-CT) has become available in clinical routine. With the ability to adjust the photon energy threshold, electronic background noise can be eliminated from image acquisition.^{9,10} The advantage of higher vessel attenuation in low-keV VMIs,^{6,11} in combination with the proven high spatial resolution¹²⁻¹⁴ and possible noise reduction, potentially permits a higher diagnostic confidence in CT angiographies. There have been some studies showing the superiority of PCD-CT concerning the radiation dose and image quality during different examinations.^{15,16} However, the possibility to improve otherwise nondiagnostic images has not been under evaluation yet.

This study analyzes the objective image quality and radiation dose of CT angiographies of the thoracoabdominal aorta with ECG-gating and a high-pitch factor performed on a PCD-CT compared with an energy-integrating detector-CT (EID-CT), with special focus on examinations with suboptimal contrast attenuation.

Materials and Methods

The Medical Research and Ethics Committee (MREC) of Ludwig Maximilian's University (Munich, Germany) approved to conduct this prospective study (protocol no. 21-0773) and the subsequent analysis of anonymized patient data. Informed consent was collected from each patient in the study group. The need for informed consent of the retrospective control group was waived by the institutional review board. The study was performed concordantly with the ethical standards of the 1946 Declaration of Helsinki and its later amendments.

Patient Population

Inclusion criteria comprised written informed consent, age ≥ 18 years, and an ECG-gated, high-pitch CTA of the thoracoabdominal aorta on a first-generation dual-source PCD-CT (NAEOTOM alpha, Siemens Healthcare GmbH, Forchheim, Germany) as part of routine clinical care between April and July 2021 (PCD-CT cohort). Exclusion criteria were missing spectral data, incomplete protocol acquisition, and missing informed consent. A control group, matched for gender, body mass index (BMI), height, and age, was selected from patients examined between January 2018 and July 2021 on a third-generation dual-source EID-CT (Somatom Definition Flash, Siemens Healthcare; EID-CT cohort). During the period when the scanners were in simultaneous clinical use, allocation to each scanner was based on availability without patient selection.

Scan Protocol and Image Reconstruction

An antecubital intravenous canula was used for contrast injection. A monophasic contrast protocol comprised an 80ml contrast material bolus (Ultravist 300, Bayer Healthcare, Berlin, Germany), followed by a 20ml of a saline chaser, both injected using a power injector with a flow of 5 ml/s. Scans were started after bolus triggering in the ascending aorta, using an enhancement threshold of 100 Hounsfield unit (HU) with a delay of 11 seconds. The scan stretched from the third cervical vertebra to the groin.

Scan protocols for both scanners were adopted from manufacturer recommendations. On the EID-CT, automated tube potential selection (ATPS; CARE kV, Siemens Healthineers) and automated tube current modulation were used (CareDose 4D, Siemens Healthineers, with reference mAs of 100, 120, and 140 kVp: 354, 320, and 312, respectively). Collimation, pitch, and rotation time were 123×0.6 , 3.2, and 0.28 seconds, respectively.

On the PCD-CT, all scans were acquired at 120 kVp, using an image quality level of 64 and a spectral acquisition mode ("QuantumPlus," Siemens Healthineers), using 4 detector-based energy thresholds (20/30/65/70 keV). Collimation, pitch, and rotation time were 144×0.4 , 3.2, and 0.25 seconds, respectively.

Medium smooth kernels and iterative reconstruction algorithms were used on both systems (I26s+ADMIRE

¹Diagnostic and Interventional Radiology, Faculty of Medicine, University Hospital Augsburg, University of Augsburg, Augsburg, Germany

²Centre for Advanced Analytics and Predictive Sciences, University of Augsburg, Augsburg, Germany

³DONAUISAR Klinikum Deggendorf, Deggendorf, Germany

*Contributed equally.

Corresponding Author:

T. J. Kroencke, Diagnostic and Interventional Radiology, Faculty of Medicine, University Hospital Augsburg, University of Augsburg, Stenglinstr. 2, Augsburg 86156, Germany.
Email: thomas.kroencke@uk-augsburg.de

3 and Bv36+QIR 3 for EID-CT and PCD-CT, respectively; Kernels and algorithms from Siemens Healthineers). These combinations had been selected for clinical routine based on their similar image texture impression. On the PCD-CT, an enhanced Digital Imaging and Communications in Medicine (DICOM) format (“Spectral Postprocessing” [SPP]) was chosen, which contains the spectral information.

All reconstructions were performed in axial orientation, using a slice thickness of 1.5 mm and an increment of 1 mm, with a manually adapted field-of-view encompassing both legs and a matrix size of 512.

The SPP reconstructions were postprocessed using commercially available software (Syngo.Via VB70A, Siemens Healthineers) to generate VMI reconstructions with identical field-of-view, matrix, and slice positioning at various keV levels (40, 45, 50, 55, 60, 65, 70, 75, 80, 90, 100, 110, and 120 keV).

Objective Image Analysis

Image analyses were performed on a dedicated workstation using commercially available (Onis 2.5, Tokyo, Japan) and open-source software (ImageJ, NIH, Bethesda, Maryland). Circular regions of interest (ROIs) were positioned in the left ventricle, the ascending aorta, the aortic arch, the descending aorta, the infrarenal aorta, and common femoral arteries. The measurements in the common femoral arteries were performed pairwise. For PCD-CT data sets, ROIs were drawn on the 70 keV VMIs and automatically copied to VMIs of all other keV levels, so that identical voxels of the data set were included (differing only in keV level),

The mean and standard deviation (SD) of CT values (HU) were derived from all ROIs as approximations for intravascular signal ($Signal_{ROI}$) and noise ($Noise_{ROI}$). For each ROI, signal-to-noise ratio (SNR) and contrast-to-noise ratio (CNR) were calculated as follows [15]:

$$SNR_{ROI} = \frac{Mean\ CT\ values_{ROI}}{SD\ CT\ values_{ROI}} \quad (1)$$

$$CNR_{ROI} = \frac{(Mean\ CT\ values_{ROI} - Mean\ CT\ values_{Psoas})}{SD\ CT\ values_{ROI}} \quad (2)$$

For each patient, the means across all ROIs for HU values ($Signal_{global}$), SDs ($Noise_{global}$), SNR (SNR_{global}), and CNR (CNR_{global}) were calculated as global descriptors of image quality on a per-patient level.

Subgroup Analysis

A subgroup analysis was performed in the study group, with the focus on patients with signs of a decreased cardiac output with a consecutively decreased velocity of blood flow in the body than in the rest of the study cohort. This was defined as

a decrease of attenuation between the ascending aorta and the femoral artery of at least 50%, which can also signify an increase of nondiagnostic scans as the femoral arteries show a decreased attenuation and may not be assessable. The aim of this subgroup analysis was to evaluate whether low-keV reconstructions raise the number of diagnostic scans in case of suboptimal attenuation at the level of the femoral arteries. Subjective image quality parameters were assessed for VMI at 40 and 70 keV in axial image reconstructions. All data sets were independently evaluated by 2 readers with 8 and 15 years’ experience, respectively. To ensure that both readers were blinded to the reconstruction and postprocessing settings, all data sets were pseudonymized and all information about the reconstruction parameters was removed. Data sets were presented in random order. Readers used a simple DICOM viewer with multi-planar reconstruction (MPR) functionality, using a window center of 40 and a width of 400, but raters were free to modify these settings as required.

Both readers independently rated vessel attenuation of the abdominal aorta, the common and external iliac artery, and the common femoral artery on a 5-point Likert scale (1 = *undiagnostic*, 2 = *poor with restricted diagnostic confidence*, 3 = *moderate diagnostic confidence*, 4 = *good diagnostic confidence*, and 5 = *excellent diagnostic confidence*). The definition for a diagnostic usable examination was a rating of 3 or above.

Statistical Analysis

Analyses were performed using R version 4.1.0 (R Foundation for Statistical Computing, Vienna, Austria). Data are presented as mean±SD or as median with interquartile range (IQR), as indicated. The normal distribution of data was assessed using the Shapiro-Wilk test. Comparisons of 2 groups of continuous variables were performed using the Student *t* test for normally distributed data and the Wilcoxon-Mann-Whitney test for nonparametric data. Categorical data were compared using the χ^2 test. The Kruskal-Wallis test with post hoc Bonferroni adjustment was used to compare multiple groups. Inter-reader agreement was assessed using Krippendorff’s alpha and interpreted as follows: 0.0–0.20 = slight; 0.21–0.40 = fair; 0.41–0.60 = moderate; 0.61–0.80 = substantial; and 0.81–1.0 = excellent. Statistically significant differences were assumed at *p* values <0.05.

Results

Patient Population

Of the initially enrolled 53 patients, 3 were excluded due to missing spectral data (n=2) or an incomplete scan (n=1). Finally, 50 consecutive patients (mean age 77.0±14.5; 31 women) were included in the PCD-CT group for subsequent analyses. The EID-CT group consisted of 50 patients who were selected, as described previously, from a group of 379

Table 1. Baseline Patient Characteristics for Both Patient Groups.

	PCD-CT cohort (n=50)	EID-CT cohort (n=50)	p value
Age, years	77.0±14.5	81.5±6.3	0.0603
Sex, female (%)	31 (62)	31 (62)	1
Weight, kg	74.6±16.4	73.8±15.7	0.8190
Height, m	1.7±0.1	1.7±0.1	0.9059
BMI, ^a kg/m ²	25.6 (23.8–29.6)	25.4 (23.9–28.6)	0.7933
Tube ct product, mAs ^a	57.0 (44.0–75.0)	349.0 (310.0–368.0)	<0.001
CTDIvol, ^a mGy	4.0 (3.1–4.9)	6.5 (5.5–9.7)	<0.001
DLP, ^a mGy ^a cm	288.0 (207.0–402.0)	466.0 (365.0–681.0)	<0.001

Data are n (%) or mean±SD or median (interquartile range).

Abbreviations: BMI, body mass index; CTDIvol, computed tomography dose index–volume; DLP, dose length product; EID, energy-integrating detector; PCD, photon-counting detector; Tube ct product, Tube current-time product.

^aNon-normally distributed.

Table 2. Mean Global Image Quality Parameters Across All Patients for the PCD-CT and EID-CT Cohorts.

keV/kVp	SignalGlobal/HU	NoiseGlobal/HU	CNRGlobal	SNRGlobal
40	1056.7±325.9	36.3±11.6	27.4±11.8	30.1±13.0
45	857.3±261.7	32.2±10.0	24.8±10.7	27.1±11.6
50	688.7±218.9	28.5±9.0	22.1±9.7	24.1±10.4
55	569.3±178.7	25.8±8.0	20.0±8.8	21.7±9.3
60	476.1±147.3	23.5±7.3	18.1±7.9	19.6±8.2
65	403.0±122.6	20.6±6.3	17.2±7.6	18.4±7.5
70	343.7±103.9	19.0±5.8	15.7±7.0	16.6±6.5
75	296.2±88.9	18.2±5.4	13.9±6.3	14.7±5.6
80	256.7±77.6	17.8±5.2	12.2±5.7	13.1±5.0
90	201.5±58.2	17.3±5.0	9.4±4.5	10.6±4.0
100	163.3±45.2	17.1±5.0	7.4±3.5	8.7±3.2
110	136.0±36.4	17.1±4.9	5.9±2.9	7.3±2.7
120	116.1±30.2	17.0±4.9	4.7±2.4	6.3±2.3
c100	369.8±133.6	21.3±11.6	19.3±12.9	21.9±12.9
c120	249.9±108.3	18.5±6.3	12.0±6.5	12.7±5.9
c140	183.7±98.8	16.9±6.4	8.4±5.4	9.3±5.3

Data are mean±SD.

Abbreviations: CNR, contrast-to-noise ratio; EID-CT, energy-integrating detector–computed tomography; HU, Hounsfield unit; PCD-CT, photon-counting detector–computed tomography; SNR, signal-to-noise ratio.

patients who had been examined on a third-generation, dual-source EID-CT. There were no significant differences between both patient groups concerning gender, age, BMI, weight, and height. Using automatic tube potential selection, 5 patients in the EID-CT cohort were scanned at 100 kVp (c100), 24 patients at 120 kVp (c120), and 21 patients at 140 kVp (c140). The computed tomography dose index (CTDI) and dose length product (DLP) were both 62% higher in the EID-CT cohort than in the PCD-CT cohort ($p<0.001$). Table 1 shows the baseline patient characteristics for both patient groups.

Objective Image Analysis

Table 2 shows the mean global image quality parameters across all patients for the PCD-CT and EID-CT cohorts. Table 3 shows the distribution of HU at the measured localizations.

The mean attenuation levels decreased with the increase of keV. In comparison with the c100 control group, the keV levels from 40 to 55 showed a significantly higher mean attenuation ($p<0.01$). When looking at the control group examined with 120 kVp, the keV levels from 40 to 70 showed a significantly higher attenuation ($p<0.01$), the keV levels at 75 and 80 showed no significant difference, and the levels above showed a significantly lower signal ($p<0.001$). Similar results were shown for the control group c140, with the tipping point being keV level 90. Furthermore, there was a significant difference between the 3 control groups in favor of the lower kVp examinations ($p<0.001$).

Image noise decreased with increasing keV levels and was significantly lower for all control groups ($p<0.05$) up to keV level 65 for c100, 75 for c120, and 90 for c140, after which the differences were no longer significant. The

Table 3. Distribution of Hounsfield Unit at the Measured Localizations.

Location	40	45	50	55	60	65	70	75	80	90	100	110	120	c100	c120	c140
Left ventricle	1078±336	877±271	704±228	584±187	490±156	416±131	356±112	308±97	268±85	213±65	174±52	147±43	127±36	312±57	192±86	137±92
Ascending aorta	1153±325	935±262	749±221	619±181	517±150	438±125	373±107	321±92	278±81	218±60	177±47	148±37	126±30	389±54	257±82	190±99
Aortic arch	1157±313	938±251	751±213	620±174	519±144	438±120	373±103	321±88	278±78	218±58	176±45	147±36	125±29	393±65	274±86	211±104
Descending aorta	1125±282	911±226	729±194	601±158	501±130	423±108	360±92	309±79	267±70	208±51	167±39	138±30	116±24	385±93	271±89	195±93
Infrarenal aorta	1070±288	866±230	694±195	571±159	476±130	401±108	341±91	292±78	252±68	196±50	157±39	129±31	109±25	387±154	280±96	202±93
Left femoral artery	898±323	730±259	592±216	490±175	411±143	348±118	298±98	257±83	224±71	176±53	144±41	120±33	103±29	359±217	230±146	170±110
Right femoral artery	903±316	734±254	595±211	493±172	414±142	352±118	302±99	261±85	227±73	180±55	147±42	123±34	106±28	365±225	233±147	162±109
Left psoas	83±41	74±31	66±24	61±18	57±14	53±12	50±10	48±9	46±9	43±9	41±10	40±11	39±12	49±6	46±10	44±9
Right psoas	80±34	71±27	63±22	58±18	54±16	50±14	48±13	45±13	44±12	41±12	39±13	38±13	37±13	53±4	47±8	43±10

Data are given as mean ±SD.

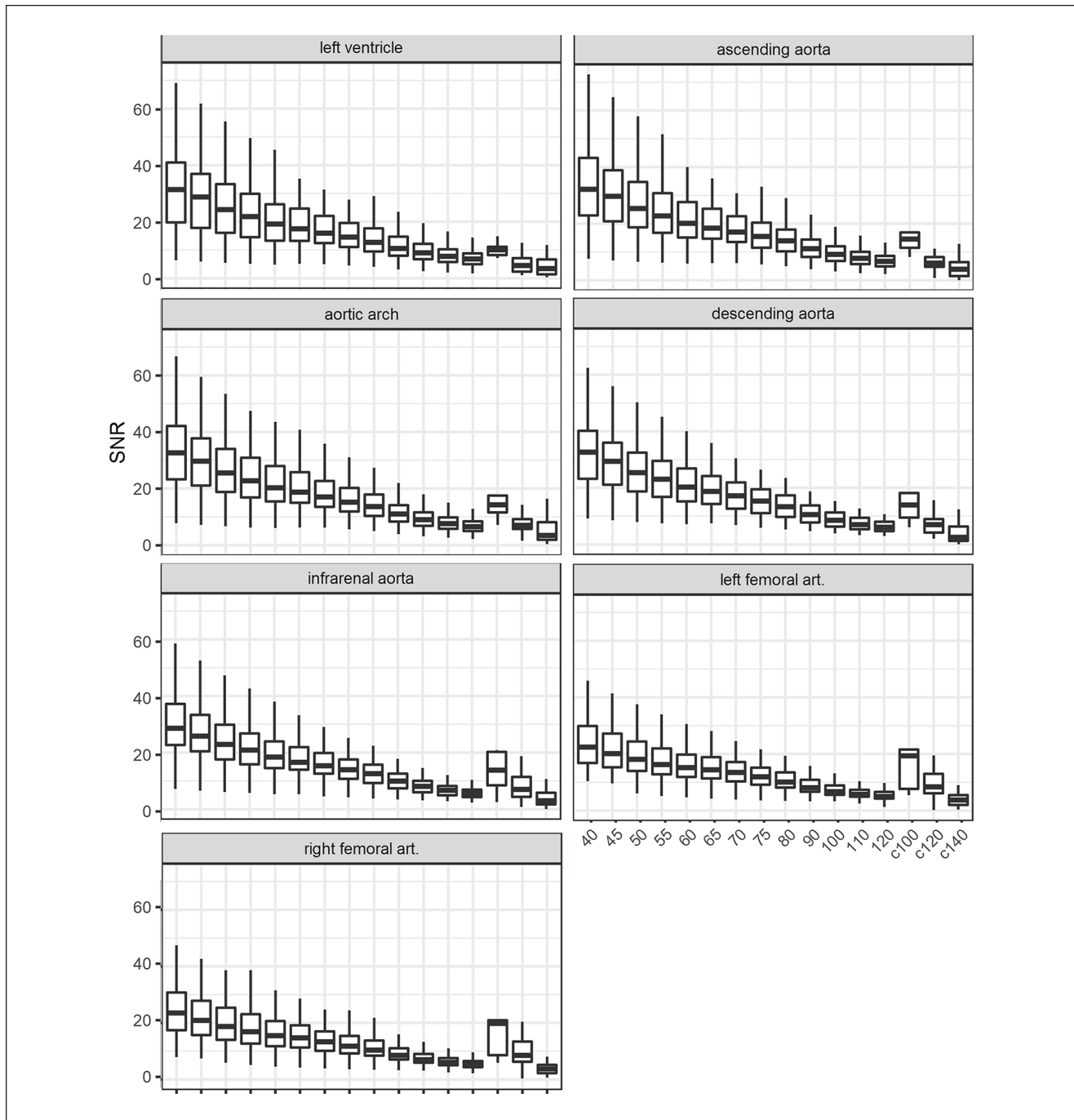


Figure 1. Results of signal-to-noise ratio comparing different keV levels of the photon-counting detector–computed tomography (PCD-CT) and both control groups of the energy-integrating detector–computed tomography (EID-CT; c80 and c100). SNR, signal-to-noise ratio.

difference of image noise between the different keV levels was highly significant ($p < 0.001$) until p increased to 0.206 between keV level 80 and 90. There was no significant difference in image noise between the control groups c100 and c120. However, there was a significant difference when comparing the 2 lower kVp control groups with the c140 control group ($p < 0.05$).

The SNR increased with decreasing keV levels (Figure 1 and Table S1). In comparison with the c100 control group, the keV levels from 40 to 50 showed no significant difference, whereas the keV levels above showed a significantly lower SNR ($p < 0.05$). When looking at the control groups c120 and c140, the keV levels from 40 to 65 and 40 to 80, respectively, showed a significantly higher SNR ($p < 0.01$).

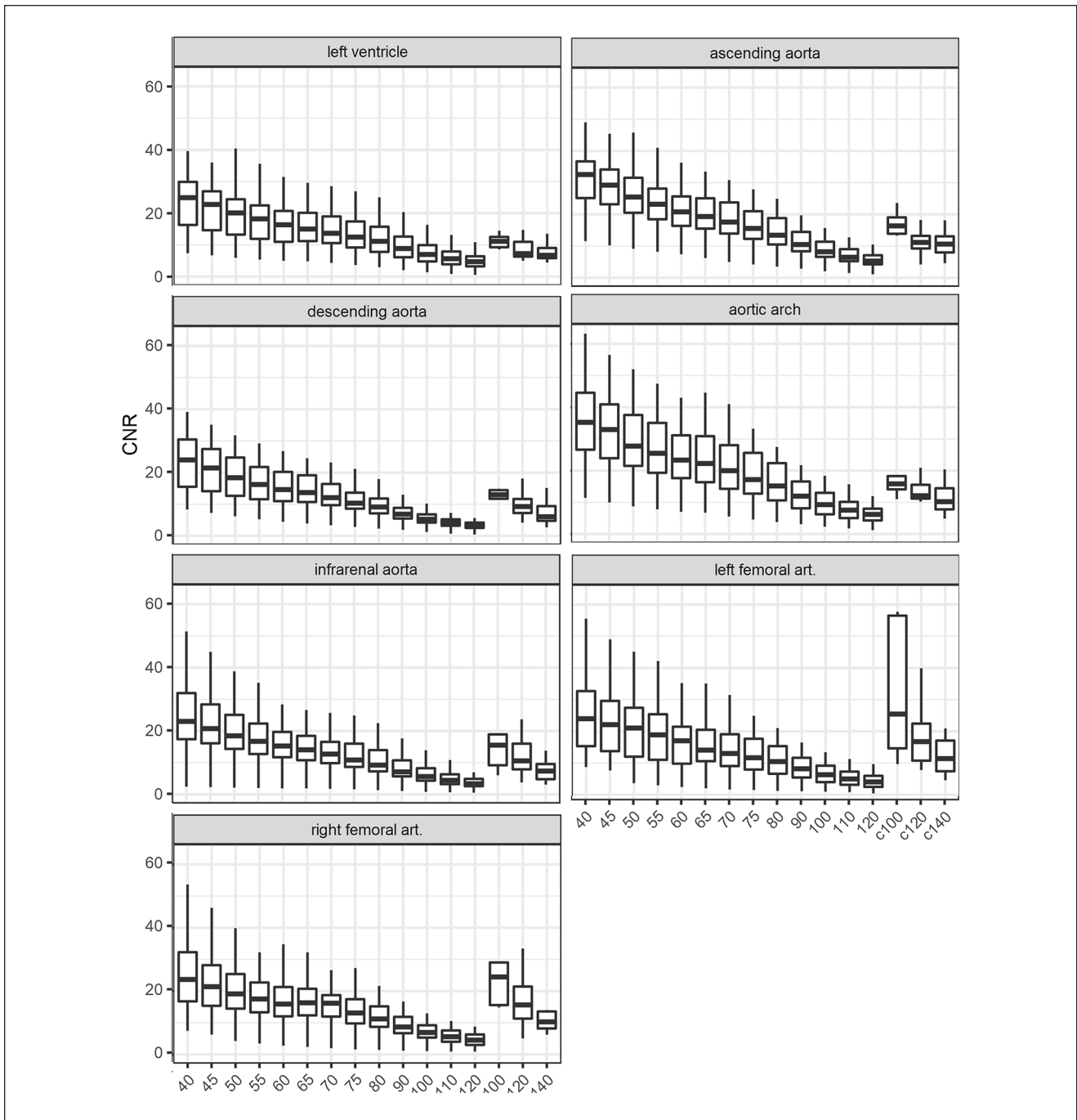


Figure 2. Results of contrast-to-noise ratio comparing different keV levels of the photon-counting detector–computed tomography (PCD-CT) and the control groups of the energy-integrating detector–computed tomography (EID-CT; c100, c120, and c140). CNR, contrast-to-noise ratio.

The differences of SNR between the 3 control groups were highly significant ($p < 0.0001$).

The CNR also increased with decreasing keV levels, as shown in Figure 2 (Supplemental Table S2). Similar to the SNR, the c100 control group showed no significant difference in the lower keV levels (40–60), whereas the

CNR decreased significantly in the keV levels above, compared with c100 ($p < 0.05$). When looking at the control groups c120 and c140, the keV levels from 40 to 65 and 40 to 75, respectively, showed a significantly higher CNR ($p < 0.005$). The differences of SNR between the 3 control groups were highly significant ($p < 0.005$).

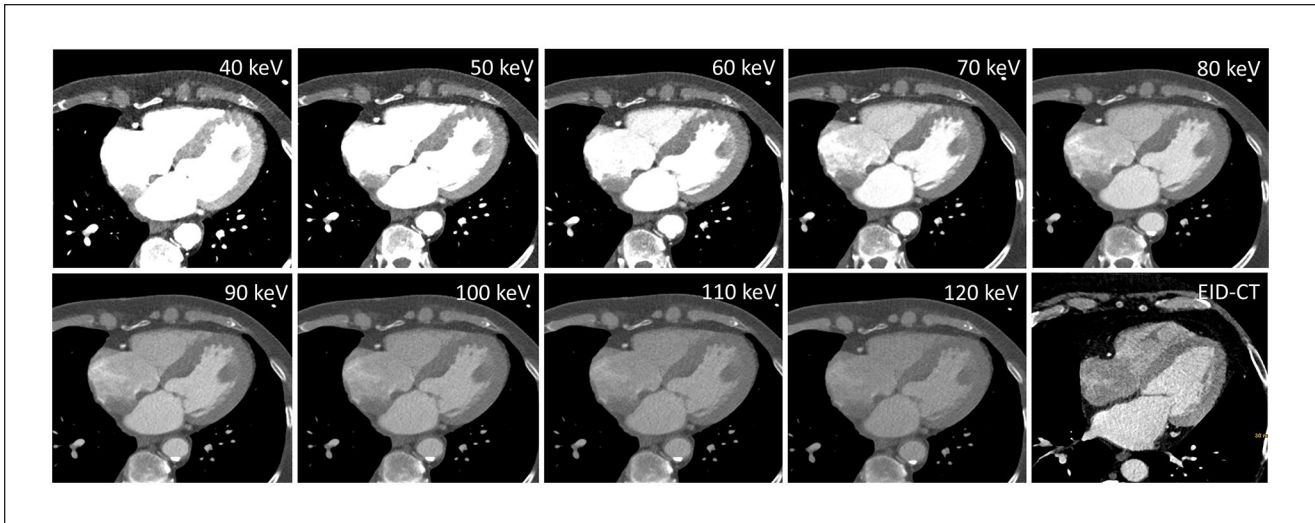


Figure 3. Example of image quality for photon-counting detector–computed tomography (PCD-CT) and energy-integrating detector–computed tomography (EID-CT). Comparison of different keV levels of a patient of the PCD-CT cohort and a patient of the EID-CT cohort.

Table 4. Results of the rating on a five-point Likert scale.

	40 keV	70 keV	p value
Aorta	4.88±0.33 5.0 (5.0–5.0)	4.29±1.00 4.5 (4.0–5.0)	0.01342
CIA ri.	4.68±1.10 5.0 (5.0–5.0)	3.76±1.11 4.0 (4.0–4.0)	<0.001
CIA le.	4.74±0.87 5.0 (5.0–5.0)	3.79±1.12 4.0 (4.0–4.5)	<0.001
EIA ri.	4.56±1.27 5.0 (5.0–5.0)	3.44±1.12 3.5 (3.0–4.0)	<0.001
EIA le.	4.62±1.22 5.0 (5.0–5.0)	3.53±1.08 4.0 (3.5–4.0)	<0.001
CFA ri.	3.94±1.60 5.0 (3.0–4.0)	2.85±1.55 3.5 (2.0–4.0)	0.01451
CFA le.	4.03±1.48 5.0 (3.5–5.0)	2.91±1.45 3.5 (2.0–4.0)	0.01186

Abbreviations: CFA, common femoral artery; CIA, common iliac artery; EIA, external iliac artery; le, left; ri, right.

Representative reconstructions of all keV levels are shown in Figure 3.

Subjective Image Analysis

Eight patients in the study group showed signs of a decreased cardiac output as defined previously. The vessel attenuation in the keV level 40 was rated significantly better than at level 70 ($p < 0.01$); the rate of acceptable diagnostic imaging improved from 50% to 75% according to the above-mentioned definition (Table 4, Figure 4). An example for the improvement of attenuation is shown in Figure 5. The

interrater agreement was excellent (Krippendorff's $\alpha = .84$).

Discussion

This study evaluated the image quality and radiation dose of high-pitch thoracoabdominal CTA of a dual-source PCD-CT in comparison with a conventional dual-source EID-CT, with special focus on the potential of VMI reconstructions to salvage studies with suboptimal contrast. The main findings of this study are the superior objective image quality of PCD-CT scans in addition to lower radiation dose. Focusing on acquisitions with suboptimal contrast in the iliofemoral arteries, low-keV VMI reconstructions could significantly increase the vascular contrast, making them usable and thus avoiding the need for repeat scans.

Using low-keV VMI, we found a significant increase of both contrast attenuation and noise, resulting in a significantly higher CNR at 40 and 45 keV, compared with the control group at the EID-CT. This concurs with Euler et al¹⁶ who also showed that the increase of noise did not influence the overall image quality in the subjective analysis significantly. Other studies have shown the same effect in various different regions of investigation.^{17,18}

Although examination protocols as similar as possible were used for both CT scanners, the ATPS at the EID-CT chose for 5 patients 100 kVp, for 24 patients 120 kVp, and for 21 patients 140 kVp. The novel PCD-CT, however, allowed spectral analysis only when conducting the examinations with a peak voltage of 120 kVp. Nonetheless, the overall radiation dose was significantly lower in the PCD-CT group ($p < 0.001$). Similar results were seen in the

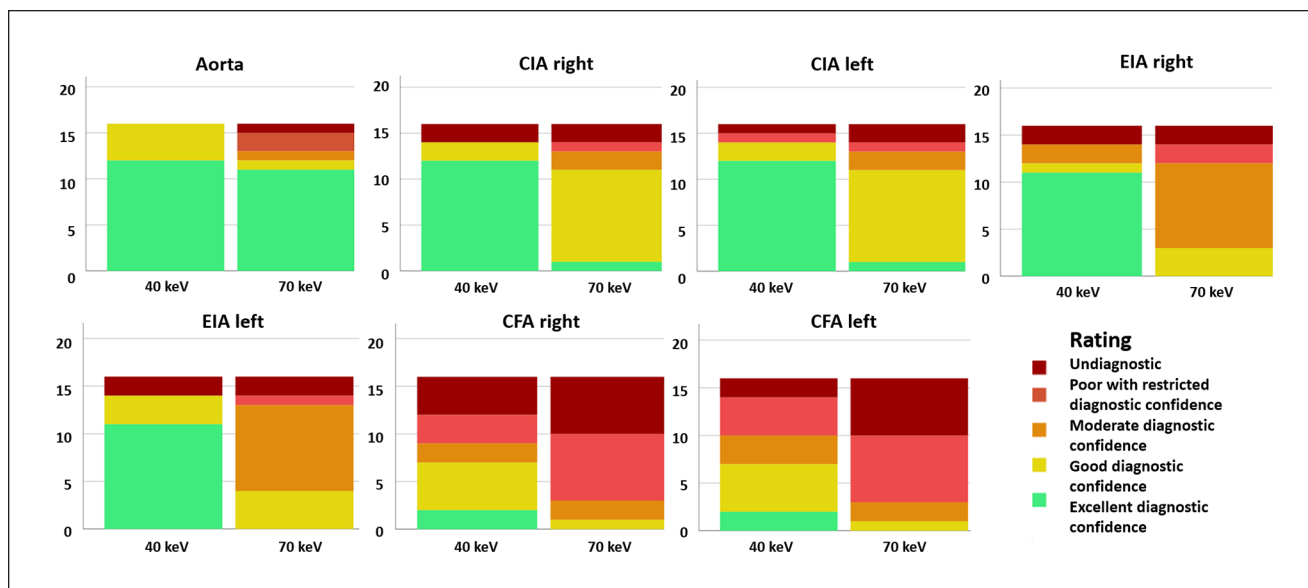


Figure 4. Results of the subjective rating at different locations for 40 and 70 keV. CFA, common femoral artery; CIA, common iliac artery; EIA, external iliac artery.

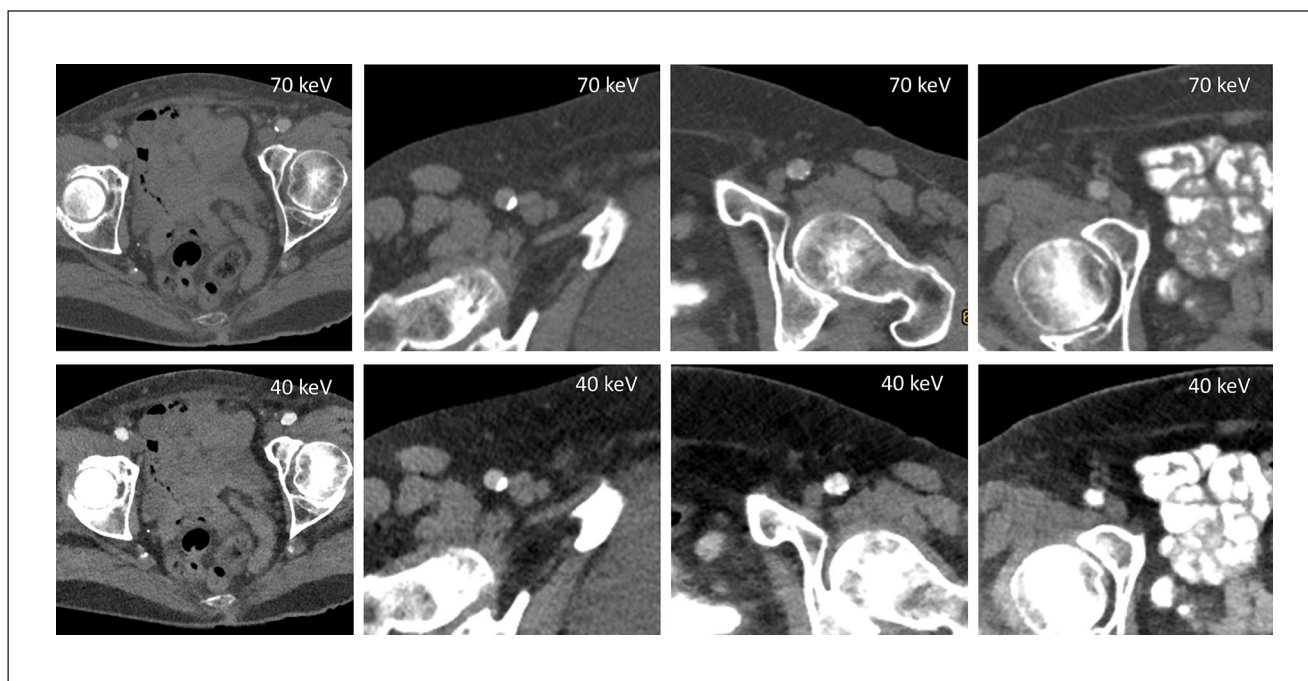


Figure 5. Examples of the improvement of contrast attenuation comparing 40 to 70 keV when looking at the common femoral artery.

study of Euler et al.¹⁶ As seen in low-keV studies on EID-CT, vascular imaging of the lower legs can be conducted at low voltage tube settings and still offer great diagnostic value.¹⁹ Wei et al.²⁰ have shown a potential for not only a decrease of radiation dose but also a simultaneous reduction of contrast medium when examining thoracoabdominal aortas with an EID-CT. There are already in vitro

studies showing the PCD-CT's potential of dose reduction using a phantom.²¹

Furthermore, there is a high potential of reducing the iodine load in low-keV VMIs. Virtual monoenergetic images have been in use since the establishment of dual-source CT scanners. As shown by Sudarski et al.,²² low-energy VMIs of EID-CT offer a better contrast attenuation,

but the diagnostic confidence also suffers from the higher noise levels. Furthermore, there were several other studies, comparing VMI of EID-CT with conventional polyenergetic images, with the same results.^{22,23} Further studies compared optimized VMIs with standard VMI.^{24,25} This optimization was created by noise-reducing reconstruction algorithms. Both studies showed an improvement of diagnostic quality in lower keV levels, but still mentioned a rise in noise levels. As seen in several studies on EID-CT, reconstructing low-keV VMIs offers the possibility of reducing the iodine load to about 50% while maintaining the radiation dose.^{26–28} However, Yoshida et al²⁹ showed a significant advantage of low kV examinations in comparison with low-keV VMIs when using a reduced iodine load.

The newest studies have shown that this principle can also be applied to PCD-CT. The decrease of noise levels due to the use of PCD-CT in low-keV reconstructions offers new possibilities for diagnostic improvement. Emrich et al³⁰ proposed a reduction of contrast media concentration of up to 50% for coronary CTA due to their results on a phantom study. However, a clinical validation has yet to be conducted. Nonetheless, in a prospective study, Higashigaito et al³¹ demonstrated a noninferior image quality of PCD-CT reconstructions at 50 keV with a contrast media volume reduction of 25% compared with EID-CT. How the aspects of dose reduction and spectral imaging in PCD-CT can and will further be combined remains to be seen.

Various studies investigated the possible benefit of PCD-CT when using VMI reconstructions due to its unique ability to lower background noise.^{15,32} The overall consent is that a VMI reconstruction of 45 to 50 keV exceedingly improves the contrast attenuation and leaves the image quality vastly unaffected. We concur with this assessment, but we do propose VMI reconstructions of 40 keV, especially when looking at low attenuation CTA. In the subjective rating of the subgroup analysis, we were able to show that, with the low-keV reconstructions, it is possible to increase the number of diagnostic acceptable scans in case of decreased contrast of approximately 50%. On one hand, this implies the possibility to decrease the overall use of contrast medium as described previously, but on the other hand it also entails the possibility to improve primary non-diagnostic images to a diagnostic level without the need to repeat the examination. This entails not only a decrease of repeat examination but also consequently reduces the iodine application for the patients. How well this retrospect amendment will work in a clinical setting has to be validated with further studies.

There are a few limitations in the setup of this study. First, this is a retrospective single-center study. Second, as mentioned previously, the lack of ability to examine patients with ATPS on PCD-CT and still obtain spectral information means that the possibility of radiation dose reduction can be further increased. Finally, subgroup analyses comprised

only a small number of patients. To confirm the findings of this study and to further assess the potential of low-keV VMI, larger prospective analyses should be performed.

In conclusion, low-keV VMIs of the thoracoabdominal CTA of PCD-CT result in significantly higher CNR and SNR than EID-CT images. We propose 40 keV reconstructions to improve diagnostic confidence, especially in cases with low-contrast attenuation, to salvage studies with sub-optimal contrast of the iliaco-femoral access route and thus reduce radiation dose by omitting repeat scans.

Declaration of Conflicting Interests

The author(s) declared the following potential conflicts of interest with respect to the research, authorship, and/or publication of this article: F.S. and the University Hospital Augsburg have received speaker honoraria from Siemens Healthcare GmbH.


Funding

The author(s) disclosed receipt of the following financial support for the research, authorship, and/or publication of this article: T.J.K. has received institutional funding.

ORCID iDs

K. Rippel  <https://orcid.org/0000-0001-5725-0973>

C. Scheurig-Muenkler  <https://orcid.org/0000-0003-0702-7460>

T. J. Kroencke  <https://orcid.org/0000-0003-4889-1036>

Supplemental Material

Supplemental material for this article is available online.

References

1. Ismail TF, Cheasty E, King L, et al. High-pitch versus conventional cardiovascular CT in patients being assessed for transcatheter aortic valve implantation: a real-world appraisal. *Open Heart*. 2017;4(2):e000626. doi:10.1136/openhrt-2017-000626.
2. Mileto A, Ramirez-Giraldo JC, Nelson RC, et al. High-pitch dual-source MDCT for imaging of the thoracoabdominal aorta: relationships among radiation dose, noise, pitch, and body size in a phantom experiment and clinical study. *AJR Am J Roentgenol*. 2015;205(4):834–839. doi:10.2214/AJR.15.14334.
3. Freyhardt P, Solowjowa N, Böning G, et al. CT-angiography of the aorta in patients with Marfan disease—high-pitch MDCT at different levels of tube voltage combined with Sinogram affirmed iterative reconstruction. *Clin Imaging*. 2018;51:123–132. doi:10.1016/j.clinimag.2018.02.007.
4. Marukawa Y, Sato S, Tanaka T, et al. Evaluating low-kV dual-source CT angiography by high-pitch spiral acquisition and iterative reconstruction in pediatric congenital heart disease patients. *Acta Med Okayama*. 2017;71(5):407–412. doi:10.18926/AMO/55438.
5. D'Angelo T, Cicero G, Mazziotti S, et al. Dual energy computed tomography virtual monoenergetic imaging: technique and clinical applications. *Br J Radiol*. 2019;92(1098):20180546. doi:10.1259/bjr.20180546.

6. Albrecht MH, Vogl TJ, Martin SS, et al. Review of clinical applications for virtual monoenergetic dual-energy CT. *Radiology*. 2019;293(2):260–271. doi:10.1148/radiol.2019182297.
7. Skawran S, Angst F, Blüthgen C, et al. Dual-energy low-keV or single-energy low-kV CT for endoleak detection? A 6-reader study in an aortic aneurysm phantom. *Invest Radiol*. 2020;55(1):45–52. doi:10.1097/RLI.0000000000000606.
8. Qiu D, Seeram E. Does iterative reconstruction improve image quality and reduce dose in computed tomography? *Radiol Open J*. 2016;1(2):42–54. doi:10.17140/ROJ-1-108.
9. Willemink MJ, Persson M, Pourmorteza A, et al. Photon-counting CT: technical principles and clinical prospects. *Radiology*. 2018;289(2):293–312. doi:10.1148/radiol.2018172656.
10. Klein L, Dorn S, Amato C, et al. Effects of detector sampling on noise reduction in clinical photon-counting whole-body computed tomography. *Invest Radiol*. 2020;55(2):111–119. doi:10.1097/RLI.0000000000000616.
11. Murphy A, Cheng J, Prata J, et al. Dual-energy computed tomography pulmonary angiography: comparison of vessel enhancement between linear blended and virtual monoenergetic reconstruction techniques. *J Med Imaging Radiat Sci*. 2019;50(1):62–67. doi:10.1016/j.jmir.2018.10.009.
12. Bette SJ, Braun FM, Haerting M, et al. Visualization of bone details in a novel photon-counting dual-source CT scanner-comparison with energy-integrating CT. *Eur Radiol*. 2022;32(5):2930–2936.
13. Leng S, Rajendran K, Gong H, et al. 150- μ m spatial resolution using photon-counting detector computed tomography technology: technical performance and first patient images. *Invest Radiol*. 2018;53(11):655–662. doi:10.1097/RLI.0000000000000488.
14. Pourmorteza A, Symons R, Henning A, et al. Dose efficiency of quarter-millimeter photon-counting computed tomography: first-in-human results. *Invest Radiol*. 2018;53(6):365–372. doi:10.1097/RLI.0000000000000463.
15. Rippel K, Decker JA, Wudy R, et al. Evaluation of run-off computed tomography angiography on a first-generation photon-counting detector CT scanner-comparison with low-kVp energy-integrating CT. *Eur J Radiol*. 2023;158:110645. doi:10.1016/j.ejrad.2022.110645.
16. Euler A, Higashigaito K, Mergen V, et al. High-pitch photon-counting detector computed tomography angiography of the aorta: intraindividual comparison to energy-integrating detector computed tomography at equal radiation dose. *Invest Radiol*. 2022;57(2):115–121. doi:10.1097/RLI.0000000000000816.
17. Booi R, van der Werf NR, Dijkshoorn ML, et al. Assessment of iodine contrast-to-noise ratio in virtual monoenergetic images reconstructed from dual-source energy-integrating CT and photon-counting CT data. *Diagnostics*. 2022;12(6):1467. doi:10.3390/diagnostics12061467.
18. Higashigaito K, Euler A, Eberhard M, et al. Contrast-enhanced abdominal CT with clinical photon-counting detector CT: assessment of image quality and comparison with energy-integrating detector CT. *Acad Radiol*. 2022;29(5):689–697. doi:10.1016/j.acra.2021.06.018.
19. Qi L, Zhao Y, Zhou CS, et al. Image quality and radiation dose of lower extremity CT angiography at 70 kVp on an integrated circuit detector dual-source computed tomography. *Acta Radiol*. 2015;56(6):659–665. doi:10.1177/0284185114535391.
20. Wei L, Li S, Gao Q, et al. Use of low tube voltage and low contrast agent concentration yields good image quality for aortic CT angiography. *Clin Radiol*. 2016;71(12):1313.e5–1313.e10. doi:10.1016/j.crad.2016.07.018.
21. Rajagopal J, Farhadi F, Solomon J, et al. Comparison of low dose performance of photon-counting and energy integrating CT. *Acad Radiol*. 2021;28(12):1754–1760. doi:10.1016/j.acra.2020.07.033.
22. Sudarski S, Apfaltrer P, Nance JW Jr, et al. Optimization of keV-settings in abdominal and lower extremity dual-source dual-energy CT angiography determined with virtual monoenergetic imaging. *Eur J Radiol*. 2013;82(10):e574–e581. doi:10.1016/j.ejrad.2013.04.040.
23. Ren H, Zhen Y, Gong Z, et al. Assessment of virtual monoenergetic images in run-off computed tomography angiography: a comparison study to conventional images from spectral detector computed tomography. *J Comput Assist Tomogr*. 2021;54(2):232–237. doi:10.1097/RCT.0000000000001126.
24. Wichmann JL, Gillott MR, De Cecco CN, et al. Dual-energy computed tomography angiography of the lower extremity run-off: impact of noise-optimized virtual monochromatic imaging on image quality and diagnostic accuracy. *Invest Radiol*. 2016;51(2):139–146. doi:10.1097/RLI.0000000000000216.
25. Leithner D, Mahmoudi S, Wichmann JL, et al. Evaluation of virtual monoenergetic imaging algorithms for dual-energy carotid and intracerebral CT angiography: effects on image quality, artefacts and diagnostic performance for the detection of stenosis. *Eur J Radiol*. 2018;99:111–117. doi:10.1016/j.ejrad.2017.12.024.
26. Alaiti MA, Attizzani GF, Fares A, et al. Contrast-sparing imaging utilizing spectral detector CT for transcatheter aortic valve replacement procedure planning. *Struct Heart*. 2020;4(3):195–203. doi:10.1080/24748706.2020.1742404.
27. Noda Y, Nakamura F, Yasuda N, et al. Advantages and disadvantages of single-source dual-energy whole-body CT angiography with 50% reduced iodine dose at 40 keV reconstruction. *Br J Radiol*. 2021;94(1121):20201276. doi:10.1259/bjr.20201276.
28. Patino M, Parakh A, Lo GC, et al. Virtual monochromatic dual-energy aortoiliac CT angiography with reduced iodine dose: a prospective randomized study. *AJR Am J Roentgenol*. 2019;212(2):467–474. doi:10.2214/AJR.18.19935.
29. Yoshida M, Nakaura T, Sentaro T, et al. Prospective comparison of 70-kVp single-energy CT versus dual-energy CT: which is more suitable for CT angiography with low contrast media dosage? *Acad Radiol*. 2020;27(5):e116–e122. doi:10.1016/j.acra.2019.07.016.
30. Emrich T, O'Doherty J, Schoepf UJ, et al. Reduced iodinated contrast media administration in coronary CT angiography on a clinical photon-counting detector CT system: a phantom study using a dynamic circulation model. *Invest Radiol*. 2023;58(2):148–155. doi:10.1097/RLI.0000000000000911.
31. Higashigaito K, Mergen V, Eberhard M, et al. CT angiography of the aorta using photon-counting detector CT with reduced contrast media volume. *Radiol Cardiothorac Imaging*. 2023;5(1):e220140. doi:10.1148/ryct.220140.
32. Yalynska T, Polacin M, Frauenfelder T, et al. Impact of photon counting detector CT derived virtual monoenergetic images on the diagnosis of pulmonary embolism. *Diagnostics*. 2022;12(1):2715. doi:10.3390/diagnostics12112715.